Dalton Transactions

ROYAL SOCIETY OF CHEMISTRY

PAPER

View Article Online
View Journal | View Issue

Check for updates

Cite this: *Dalton Trans.*, 2025, **54**, 10270

The ternary C@Al_6Cu_4 cluster: hexavalent non-hybridized carbon atoms and a new magic number†

Yassin A. Jeilani,[a] Long Van Duong, *[b,c] Nguyen Minh Tam [d] and Minh Tho Nguyen [c,e]

Received 28th December 2024,
Accepted 21st May 2025

DOI: 10.1039/d4dt03563a

rsc.li/dalton

This study investigates the stability of C@Al_6M_4 structures, where six Al atoms surround a central carbon in octahedral C@Al_6, and coinage metal M (Cu, Ag, or Au) atoms attach to the four faces of C@Al_6, forming a tetrahedral shape. These structures exhibit aromaticity and significant thermodynamic stability. Their stability is compared with that of C@Al_6Na_4 and explained through the new magic number of 26. The separation of the 2P and 1F energy levels is attributed to this magic number. Carbon utilizes both its 2s and 2p orbitals for bonding, yet no hybridization is observed. Additionally, C@Sn_6^{2+}, adhering to the new magic number of 26, is also reported in this study. The concept of *"hexavalent non-hybridized carbon atom"* is applied to all the abovementioned structures.

1 Introduction

According to the classical octet rule, which was proposed by Lewis in 1916, atoms prefer having eight electrons in their valence shell to achieve a stabilized electronic configuration similar to that of the closest noble gas. Like other empirical rules of thumb in chemistry, the octet rule is not valid for some elements, but it remains popular among chemists and helps in understanding the bonding behavior of many elements.

For the carbon atom, the octet rule is established to be predominant and almost self-evident in organic compounds and also in most carbon-containing compounds. In planar structures, carbon predominantly employs sp^2 hybridization, corresponding to a coordination number of three. Some well-known cases that have drawn attention to carbon include planar tetracoordinate carbon, corresponding to a coordination number of four in cases such as the perfect D_{4h} C@E_4^{2-} (E = Al, Ga, In, and Tl)[1] and planar pentacoordinate carbon, with a coordination number of five in cases such as the perfect D_{5h} C@Cu_5H_5,[2] C@$Be_5Au_5^+$,[3] and C@Al_5^+.[4] In three-dimensional configurations, sp^3 hybridization leads to a coordination number of four. This makes perfect, highly symmetric structures with coordination numbers greater than four particularly remarkable. The perfect highly symmetric structure means that C is bonded to the nearest M atoms with equal C–M bond lengths. C@Si_8^{2+} is a perfectly cubic structure in which carbon is equally bonded to all eight silicon atoms.[5] Octahedral [C@$(AuL)_6$]$^{2+}$ structures have been synthesized, featuring six Au atoms surrounding a carbon atom in an octahedral arrangement, stabilized by various ligands (L).[6–10] Notably, MO analysis has revealed that C participates in bonding with Au through an extremely rare non-hybridized form. Specifically, the 2s orbital of C overlaps with the 1S-shape of Au_6, while the 2p orbital of C overlaps with the 1P-shape of Au_6, without any hybridization between the 2s and 2p orbitals of C.[6] The CAu_6^{2+}, which is already stable according to the jellium model[11] with eight electrons, becomes even more stabilized due to this unique hybridization. Another case where C binds perfectly with six surrounding Al atoms is the tetrahedral CAl_6Na_4,[12] and the number of electrons in this case was reported as a "new magic number of 26". In this study, we replace four Na atoms with coinage metal atoms to investigate the influence of these dopant atoms on the stability of the cluster with a "new magic number of 26". Additionally, we utilize the non-hybridization of C to elucidate the underlying mechanism responsible for the formation of this "new magic number of 26".

[a]*Department of Chemistry, University of Hail, Hail, Saudi Arabia*
[b]*Atomic Molecular and Optical Physics Research Group, Science and Technology Advanced Institute, Van Lang University, Ho Chi Minh City, Vietnam.*
E-mail: duongvanlong@vlu.edu.vn
[c]*Faculty of Applied Technology, School of Technology, Van Lang University, Ho Chi Minh City, Vietnam*
[d]*Faculty of Basic Sciences, University of Phan Thiet, 225 Nguyen Thong, Phan Thiet City, Binh Thuan Province, Vietnam*
[e]*Laboratory of Chemical Computation and Modeling, Institute for Computational Science and Artificial Intelligence, Van Lang University, Ho Chi Minh City, Vietnam*

†Electronic supplementary information (ESI) available: Partial and total densities-of-states (DOS), the overlap population density-of-states (OPDOS) of C@Al_6Ag_4, C@Al_6Au_4, and C@Al_6Na_4. See DOI: https://doi.org/10.1039/d4dt03563a

Of the coinage metals, only Au derivatives were extensively synthesized in structures encapsulating a C atom,[6–8,13,14] and this structural type is classified as "Schmidbaur gold – $[E(AuL)_n]^{m+}$".[15] In contrast, both Ag and Cu encounter greater difficulty in encapsulating a C atom. The tetrahedral geometry[16–18] is intriguing as it serves as a crucial bridge in building blocks during the assembly of larger molecules or crystals. For the "magic number of 2", the tetrahedral Au_4^{2+} has extensively been synthesized thanks to ligand stabilization.[19–22] While a similar geometry of Ag_4^{2+} has been stabilized in zeolites,[23] no experimental evidence of such a structure has been found yet for Cu_4^{2+}. Similarly, for the "magic number of 20", the highly stable Au_{20}, which adopts a tetrahedral structure,[24] has also been successfully synthesized.[25,26] A distortion to a lower point group than T_d has been observed in Ag_{20} and Cu_{20},[27] and to date, no experimental synthesis has been reported for the latter.

In this context, we set out to explore methods for stabilizing a C@M_n unit, where the carbon atom exhibits six-fold valency and hexa-coordination, utilizing quantum chemical computations. Following extensive searches, we focused on the C@Al_6 unit and we found that a set of four Cu atoms can effectively stabilize the C@Al_6 unit where the resulting C@Al_6Cu_4 exhibits exceptionally high thermodynamic stability and, perhaps more interestingly, a non-hybridized central carbon atom. Moreover, the inherent stability due to the magic number of 20 electrons of Al_6^{2-} [28] is preserved through an entirely novel bonding mechanism, which is characterized by a new magic electron number. An inverse effect is observed when copper atoms are replaced by larger coinage metal congeners including silver and gold atoms, which consistently lead to a reduction in the stability of the hexavalent structure.

2 Computational methods

The search for a global minimum structure[29] is carried out using a combination of the random kick algorithm[30] and the genetic algorithm.[31] The structures generated by both algorithms are initially optimized using the density functional theory method with the revTPSS[32] functional and the def2-TZVPD[33] basis set, without vibrational frequency calculations. All optimized structures with energies ranging within 3 eV of the most stable structure are then re-optimized, and their harmonic vibrational frequencies are calculated using the revTPSS[32] and the B3LYP[34–36] functionals in conjunction with the def2-TZVPPD[33] basis set. For the CAl_6 isomers, single-point electronic energy calculations are performed using coupled cluster theory, CCSD(T),[37] and multi-configurational methods, CASSCF(12,12)/CASPT2,[38,39] with the aim of verifying the reliability of the results obtained from the applied density functionals.

The GIMIC 2.0 [40] program is used to calculate the gauge-including magnetically induced current (GIMIC).[41] The direction of current flow was analyzed to determine the diatropic (clockwise) or paratropic (counterclockwise) characteristics of the ring current. The Multiwfn program[42,43] was used to calculate the density-of-states (DOS), and the overlap population density-of-states (OPDOS). The atomic charge and electronic configuration were calculated using the NBO7 package.[44] Except for CASSCF, which was computed using Orca 6.0,[45] all other calculations were performed using the Gaussian 16 program.[46]

SEAGrid (https://seagrid.org)[47,48] is acknowledged for computational resources and services for the results presented in this publication.

3 Results and discussion

For CAl_6Au_4, there is a competition in stability between the 2D and 3D structures. However, we lack sufficient HPC resources to perform post-HF calculations to verify the reliability of DFT functionals in this case. A common approach is to conduct benchmarking on a smaller molecule. In this study, we selected CAl_6 as it falls within our computational capacity for CCSD(T) calculations and provides insight into molecular development. The revTPSS functional has been widely employed to determine the stable structures of transition metal-containing molecules[49,50] and has been benchmarked as highly reliable.[51] However, when performing structural stability searches, B3LYP tends to overestimate the stability of the 2D form.[52,53] B3LYP is a classical functional that remains widely used to this day.[54,55] Here, we once again demonstrate that B3LYP often overestimates the stability of 2D materials relative to their 3D counterparts, as evidenced by comparisons with revTPSS, CCSD(T) and CASSCF(12,12)/CASPT2 results.

3.1 The CAl_6 cluster

Although CAl_6 has previously been explored,[56] we re-examined this cluster in order to clarify certain issues that are essential for the main findings of this present study. The most stable isomers of CAl_6 are presented Fig. 1.

The three isomers that Yang and co-workers considered[56] to have degenerate energy include the **CAl_6·1**, **CAl_6·3** and **CAl_6·4** isomers displayed in Fig. 1. Additionally, we found a new isomer, **CAl_6·2**, whose energy is not significantly different from that of **CAl_6·1** and this isomer was not located in ref. 56. **CAl_6·2** actually features carbon bonded to five Al atoms and is considered a deviation from the expected perfect C@Al_6 structure. When optimized using the revTPSS functional, **CAl_6·3** spontaneously rearranges into **CAl_6·2**, implying that **CAl_6·3** is not a local minimum by this functional. The next two isomers are **CAl_6·5** and **CAl_6·6**, with **CAl_6·6** being a planar structure; this is of particular significance for the subsequent results. The planar structure **CAl_6·6** is only 5.9 kcal mol^{-1} higher in energy than **CAl_6·1** by B3LYP calculations, but this difference increases to 28.7 kcal mol^{-1} following the revTPSS calculations. The CCSD(T) method is employed to assess the accuracy of the functional's results, with a difference of 20.1 kcal mol^{-1}, thus indicating the suitability of the revTPSS functional. However, the $T1$ values of the CCSD wavefunctions exceed the value of 0.03, suggesting that the

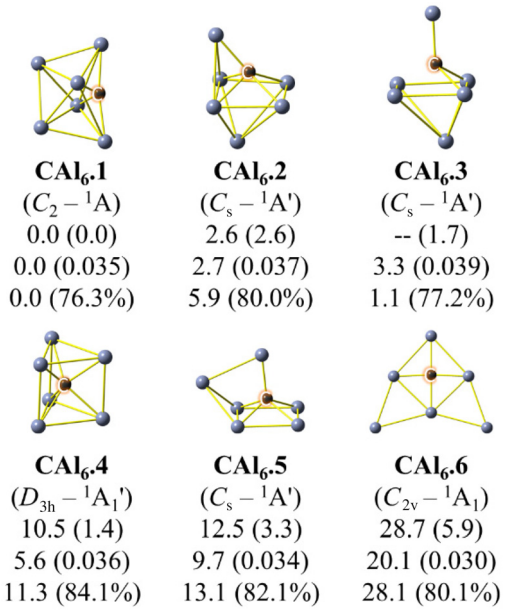

Fig. 1 Relaxed geometries of CAl_6 isomers with their symmetry point group and electronic state. Relative energies (given in kcal mol^{-1}) are obtained with ZPE corrections without frequency scaling at the respective functional, revTPSS and B3LYP (parentheses) in conjunction with the def2-TZVPPD basis set. Relative energies obtained by single-point electronic energies at CCSD(T)/def2-TZVPPD (and *T*1 value) are given in the fourth row, and relative energies obtained by CASSCF(12,12)/CASPT2 energies (and weight of the ground state configuration) energies are given in the fifth row.

CCSD(T) values also need to be regarded with caution.[57] The CASSCF(12,12)/CASPT2 calculations appear to support the values obtained by the CCSD(T) method. The multi-configurational results show that **CAl6·6** is less stable than **CAl6·1** by up to 28.1 kcal mol^{-1}. The configuration interaction (CI) weights of the main references identified from the CASSCF wavefunction range from 75 to 85%, indicating a certain degree of multireference character in these isomers. The comparable relative energies between CCSD(T) and CASSCF/CASPT2 results point out that DFT results can be trusted to a certain extent with the revTPSS functional. For its part, the B3LYP functional significantly overestimates the stability of 2D structures as compared to their 3D counterparts, as it has been demonstrated in previous studies.[52,53]

3.2 The $C@Al_6M_4$ clusters with M = Cu, Ag, Au and Na

We now examine the effects of four metal atoms M on the isomeric structures of the $C@Al_6$ unit. The most stable isomers of CAl_6M_4 with M = Cu, Ag, Au and Na are presented in Fig. 2. The various isomers of CAl_6M_4 are denoted in the format **M·A**, where **M** = **Cu**, **Ag**, **Au**, or **Na** represents the substituted metal in CAl_6M_4, and **A** = **1**, **2**, **3**, ..., corresponds to the increasing order of their relative energies compared to the lowest-energy isomer.

At first glance, when using the revTPSS functional, the global energy minima of all these tertiary clusters exhibit a tetrahedral metal-coordinated octahedral $C@Al_6$ framework, namely $C@Al_6M_4$ (corresponding to **M·1**). The quasi-planar structure **Au·6** has a quasi-planar CAl_6Au_3 frame and a fourth Au atom is positioned above the plane, connected to three Al atoms, and it becomes the most stable isomer, as determined by B3LYP functional calculations. However, it becomes less stable than the T_d **Au·1** structure by 12.6 kcal mol^{-1} at the revTPSS functional. The most stable isomers of CAl_6Na_4 presented in Fig. 2 are in complete agreement with those of the previous report by Tang *et al.*[12] The T_d **Na·1** was subsequently utilized by Zhou and co-workers as an assembly cluster to develop a superlight Zintl phase semiconductor.[58]

The most notable similarity between CAl_6Na_4 and CAl_6Cu_4 is that the six most stable isomers, as shown in Fig. 2, all represent different arrangements of Na or Cu atoms around the antiprismatic $C@Al_6$ core. In contrast, **Ag·5** exhibits a prismatic configuration of $C@Al_6$ with relative energy as high as 22 kcal mol^{-1} compared to **Ag·1**. The prismatic form of $C@Al_6$ emerged earlier in the CAl_6Au_4 series, appearing in **Au·4** with only a 9.6 kcal mol^{-1} energy difference compared to **Au·1**. Notably, **Au·3** adopts the geometry of the $C@Al_6$ core that is neither antiprismatic nor prismatic. In the case of the **Au·2** isomer, one Au atom is bonded to only two Al atoms, as opposed to three, as observed in the corresponding isomers of CAl_6Na_4, CAl_6Cu_4, and CAl_6Ag_4. This preference of Au for bonding with two Al atoms contributes to the stability of the quasi-planar geometry found in **Au·6**.

Based on the relative energy values of these clusters with respect to the second most stable isomer, their relative stabilities can be ranked in the order **Cu·1** > **Ag·1** > **Na·1** > **Au·1**. Another parameter commonly used to compare the stability of different molecules is the HOMO–LUMO gap (HLG). The HLG values for **Cu·1**, **Ag·1**, **Au·1** and **Na·1** amount to 3.2, 2.8, 2.2 and 2.8 eV, respectively, corresponding to the highest stability for **Cu·1**, the lowest for **Au·1**, while both **Ag·1** and **Na·1** exhibit comparable stability. The following analysis of chemical bonding demonstrates why such comparisons of stability are justified.

3.3 Chemical bonding

The MO analysis is first conducted to reveal the intrinsic bonding nature of the $C@Al_6M_4$ clusters. Fig. 3 presents the MO energy levels of $C@Al_6M_4$ compared to those of Al_6^{2-}. Due to the splitting of the D and F electron shells into smaller subshells, these subshells are designated a, b, c... in order to compare their energy levels in both Al_6^{2-} and $C@Al_6M_4$; the MOs are assigned following the convention in Al_6^{2-}. The energy levels presented in Fig. 3 demonstrate that the stability of the $C@Al_6M_4$ clusters arises from the MOs associated with the electron shell [$1S^2$ $1P^6$ $2S^2$ $1D^{10}$ $2P^6$], consistent with the view of a "*new magic number of 26*",[56] which differs from the shells of 20 or 40 electrons of the standard jellium model. The jellium model[11] features an electronic configuration of [$1S^2$␣$1P^6$␣$1D^{10}$_$2S^2$␣$1F^{14}$_$2P^6$␣$1G^{18}$ ...], where the "_" symbol represents two shells with closely or even overlapping energy levels, and the "␣" symbol represents two shells immediately adjacent to it with significantly separated energy levels.[59]

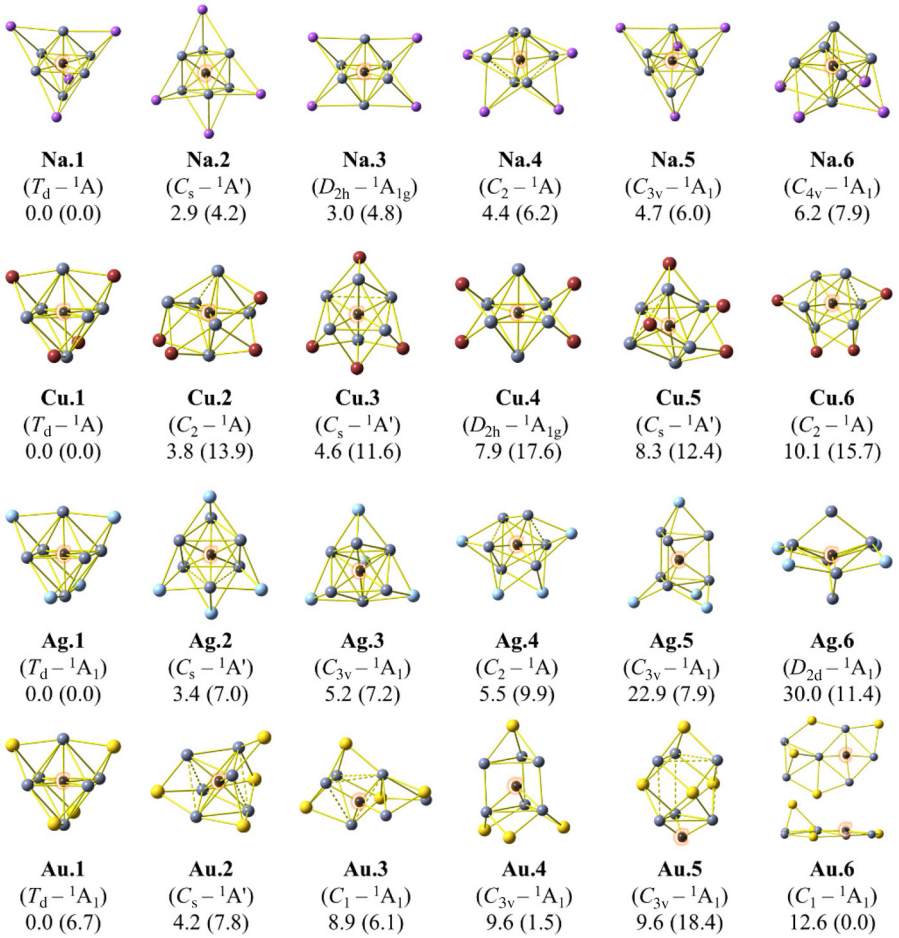

Fig. 2 Relaxed geometries of the CAl_6M_4 cluster with their symmetry point group and electronic state, M = Cu, Ag, Au, and Na. Relative energies (kcal mol^{-1}) are obtained with ZPE corrections without frequency scaling at revTPSS and B3LYP (parentheses) functionals in conjunction with the def2-TZVPPD basis set.

Energy gaps between the 2S and 1F shells, as well as between the 2P and 1G shells, lead to the magic numbers 20 and 40 of the jellium model. Thus, the significant downward shift of the 2S level as compared to 1D in $C@Al_6M_4$ (*cf.* Fig. 3) is an intriguing observation, which can be noted as a primary feature. This point will be analyzed in detail subsequently in this section.

Another noteworthy point is that the 2P subshell is characterized by a considerably lower energy as compared to the 1F subshell in $C@Al_6M_4$. This leads to the emergence of the magic number of 26 for the series of $C@Al_6M_4$ compounds. However, the significant downward shift of the 2P level, as compared to 1F, is not primarily caused by the presence of the C atom inside the Al_6 cage. It is also not due to the view that "*the central* C^{4+} *carrying a larger charge depresses the potential locally*" as mentioned in a previous paper.[12] In fact, even in pure Al_6^{2-}, its triply degenerate LUMO+1, corresponding to the 2P subshell, is already observed to have an energy lower than that of the $1F_a$ subshell by up to 1.9 eV (*cf.* Fig. 3). The higher energy MOs have more nodal planes, and as a consequence, two conditions are required for their formation, namely, either the use of AOs from higher-lying shells, which inherently possess more nodal planes, or a multi-layered structure which creates nodal planes between the layers, or both conditions. The 1F subshell in the high symmetry O_h Al_6^{2-} is formed *via* the former path as it consists of only a single layer. As a result, the 2P subshell primarily arises from the contributions of 3p atomic orbitals (AOs) of Al atoms, while the 1F subshell requires contributions from 4d AOs of Al atoms that are located at higher energy. Here, uppercase letters such as S, P, D, *etc.*, are used for molecular orbitals (MOs), while lowercase letters such as s, p, d, *etc.*, are used for atomic orbitals (AOs) from individual atoms. We attempt to theoretically determine the most stable form of the poly-anion Al_6^{8-}. Interestingly, while only the O_h isomer, where the 2P subshell is fully occupied, converges into the O_h equilibrium structure without imaginary frequency, all other initial isomers undergo fragmentation due to excess electrons. Thus, the contributions of 8 valent electrons from one C and four M atoms tend to neutralize Al_6^{8-} to form $C@Al_6M_4$ without altering the number of delocalized electrons. Nevertheless, this does not imply that the 26 delocalized electrons could guarantee the stability of

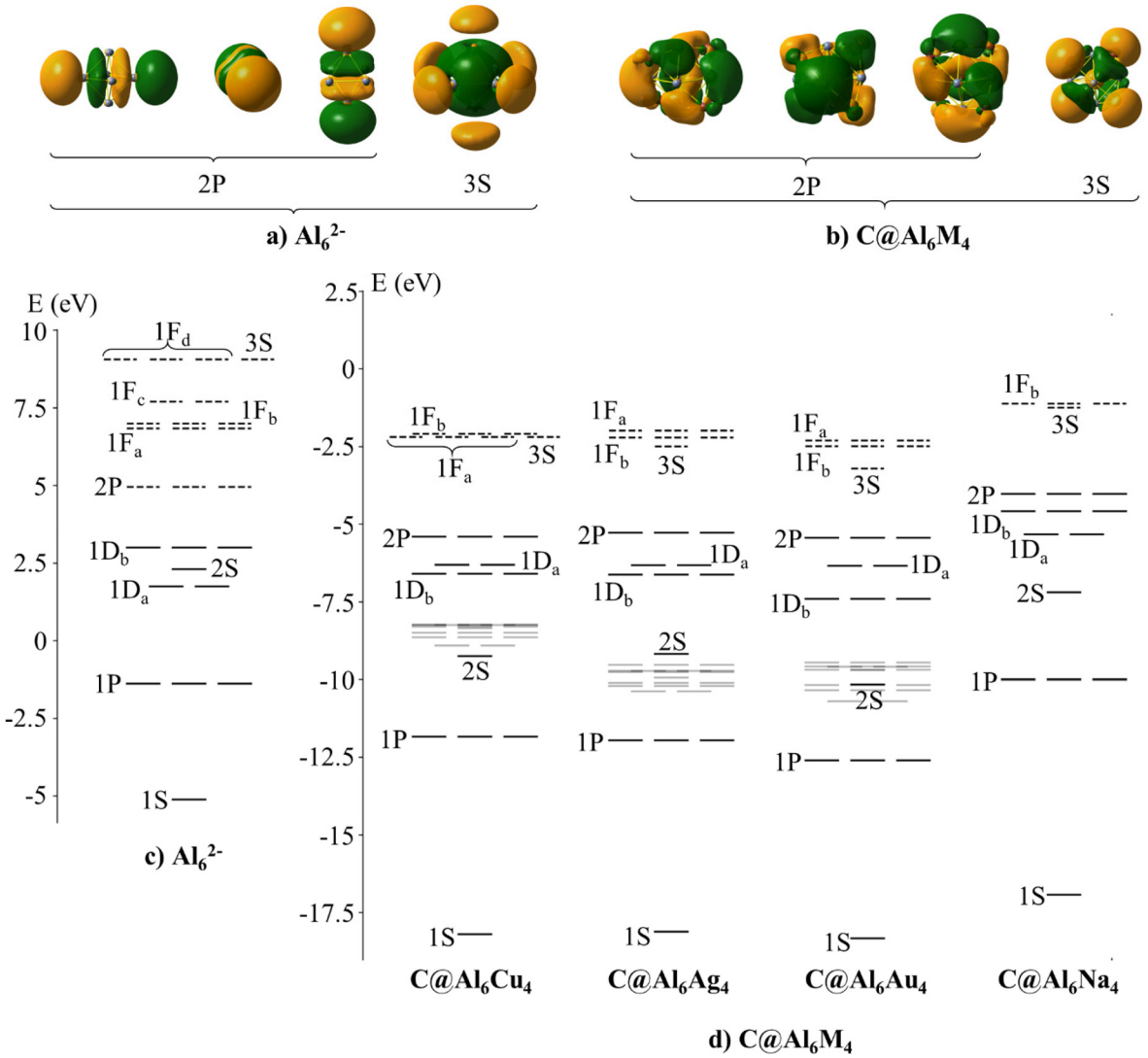

Fig. 3 Molecular orbital energy levels at B3LYP/def2-TZVPPD for (c) Al_6^{2-} and (d) $C@Al_6M_4$ with M = Cu, Ag, Au, and Na. The lines and dashed lines correspond to the occupied and unoccupied MOs. The grey lines belong to the d-AO band of coinage metals. (a) and (b) are the selected MOs visualized for Al_6^{2-} and $C@Al_6M_4$, respectively.

the O_h Al_6 framework. Indeed, when examining the O_h structure for the Al_6M_8 unit, we find that this binary cluster is either less stable or even entirely unstable. The Al_6M_8 configuration features two atomic layers, resulting in the 1F subshell having lower energy. This significantly reduces the HOMO–LUMO gap, which corresponds to the separation between both the 2P and 1F subshells.

The densities-of-states (DOS) and the overlap population density-of-states (OPDOS) of **Cu·1** are shown in Fig. 4, whereas those of other $C@Al_6M_4$ are shown in the ESI.† The pDOS (the partial densities-of-states) for s and p AOs from C, are significantly smaller as compared to the pDOS of Al and M. Therefore, the pDOS of s and p AOs from C are doubled and plotted downward to better illustrate their contribution. Similarly, for the overlap population density-of-states (OPDOS), the degree of overlap for all OPDOS, except for the Al and M overlap, is multiplied by a factor of 5. Positive OPDOS values are highlighted in blue, while negative ones are shown in red.

There is no significant difference in the contributions of the AOs from Al, M, the s orbital of C and the p orbital of C in the DOS plots for all $C@Al_6M_4$ clusters. The s(C), being the s orbital from C, overlaps with those of Al and M atoms in the 1S and 2S MOs, while the p(C), being the p orbital of C, overlaps with Al and M in the 1P, $1D_b$ and 2P MOs. It means that any MO involving contributions from s(C) orbitals shows no contributions from p(C) orbitals, and *vice versa*. In fact, the p_x, p_y, and p_z orbitals are mutually orthogonal, providing the most favorable condition for hybridization with the six atoms at the vertices of an octahedral structure. Any hybridization between the s and p orbitals, regardless of the ratio, will reduce this symmetry, making perfect hexa-coordinate symmetry unattainable. Consequently, the OPDOS between s(C) and p(C) turns

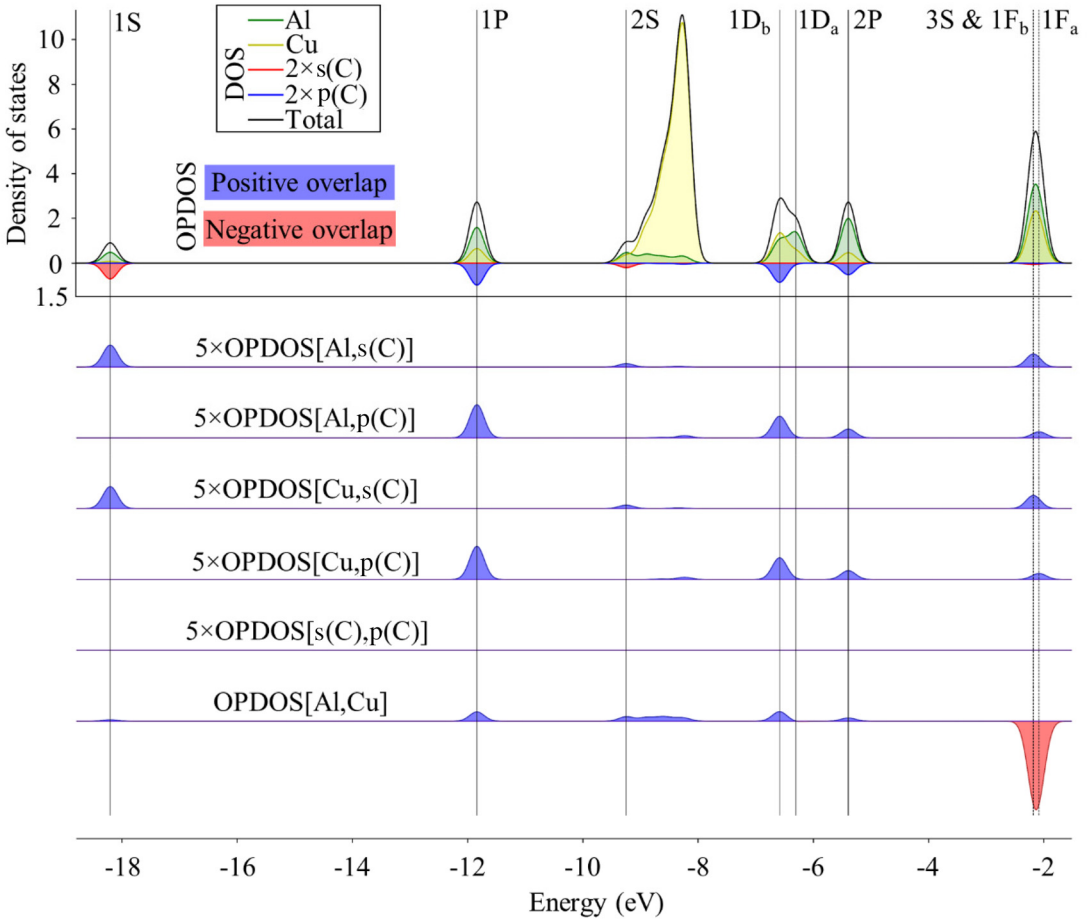

Fig. 4 The partial and total densities-of-states (DOS) and the overlap population density-of-states (OPDOS) of C@Al_6Cu_4.

out to be always equal to zero, indicating the absence of hybridization between both s and p AOs of C. In other words, the C atom in C@Al_6M_4 is non-hybridized.

Table 1 presents the atomic charges and electronic configuration of the C, Al and M atoms in the ternary C@Al_6M_4 molecules. Using the AIM method, Tang *et al.*[12] reported that C in **Na·1** carries a charge of $-4.7|e|$, indicating that Al and Na excessively donate electrons to C beyond the electronic configuration of the noble gas neon. In this study, the atomic charge of C amounts to $-3.0|e|$, as determined by the NBO7 method, which provides a more realistic value. Indeed, in all C@Al_6M_4 species considered, the 2p orbital of C is nearly fully occupied, while the 2s orbital loses approximately 0.5 electrons because of its overlap with the metal orbitals. This reinforces the overlap between the p_x, p_y, and p_z AOs of C with the P_x, P_y, and P_z MOs of the Al_6M_4 framework, which plays a more significant role in the bonding between carbon and the outer atoms than the overlap between the s AO and other MOs. As a result, C becomes a negatively charged center forming ionic bonds with external positive ions, except for Al in **Na·1**. In the latter, each Na atom donates nearly 1 electron to C, forming the polarized $C^{-3.0}[Al_6]^{-0.2}[Na_4]^{+3.2}$ structure; in reality, six Al atoms almost act as six neutralizing molecular units. The behavior of coinage metals differs from that of alkali metals. Coinage metals, together with Al, donate an equal amount of electrons as much as possible to C. Cu and Ag contribute nearly the same amount of electrons (to form $C^{-3.1}[Al_6]^{+1.2}[M_4]^{+1.9}$), while Au is less inclined to donate electrons (to form $C^{-3.1}[Al_6]^{-2.0}[Au_4]^{+1.0}$). Consequently, **Au·1** becomes significantly less stable.

Table 1 Atomic charges, summary of atomic charges (of Al and M), and the electronic configuration of C, Al and M atoms in C@Al_6M_4

Species	C	Al	M
Cu·1	−3.07 $[He]2s^{1.56}2p^{5.47}$	0.20 (1.17) $[Ne]3s^{1.43}3p^{1.31}$	0.48 (1.90) $[Ar]4s^{0.56}3d^{9.93}$
Ag·1	−3.07 $[He]2s^{1.56}2p^{5.47}$	0.19 (1.16) $[Ne]3s^{1.43}3p^{1.32}$	0.48 (1.91) $[Kr]5s^{0.56}4d^{9.93}$
Au·1	−3.07 $[He]2s^{1.55}2p^{5.48}$	0.24 (2.01) $[Ne]3s^{1.40}3p^{1.20}$	0.35 (0.97) $[Xe]6s^{0.86}4d^{9.87}$
Na·1	−3.02 $[He]2s^{1.54}2p^{5.41}$	−0.04 (−0.21) $[Ne]3s^{1.47}3p^{1.52}$	0.81 (3.24) $[Ne]3s^{0.19}$

The OPDOS value emerges as an effective indicator for understanding the above ranked stability of C@Al_6M_4. **Cu·1** is a special case where all the listed fragment AOs exhibit positive OPDOS, indicating that all these AOs join to form bonding overlaps. This leads to the higher stability of **Cu·1** as compared to **Ag·1**, **Au·1** and **Na·1**. The OPDOS indicates that the overlap between two fragments is antibonding. In **Ag·1**, Ag and p(C) are the most strongly antibonding fragments of the $1D_b$ subshell. At the 2S shell, there is a small antibonding interaction between Ag and s(C) and a weaker antibonding between Al and s(C). Considering the sign of OPDOS for all AO-fragment pairs in the 13 delocalized MOs, **Ag·1** and **Na·1** are entirely similar. However, the OPDOS[Al,s(C)] of **Na·1** is significantly more negative as compared to that in **Ag·1**. Since the bond formed between C and Al is more significant than the bond between C and M, the increased degree of antibonding overlaps in OPDOS[Al,s(C)] offers the main reason for **Na·1** being less stable than **Ag·1**. Finally, **Au·1** exhibits the least stability due to the presence of negative OPDOS at the two highest occupied energy levels (HOMO and HOMO−1), specifically OPDOS[Al, Au] in the $1D_a$ subshell and OPDOS[Al,p(C)] in the 2P subshell.

The molecular magnetically induced currents of the ternary C@Al_6M_4 clusters are shown in Fig. 5. Since all subshells that have occupied MO levels are fully filled, the aromaticity demonstrated by the ring current maps evidently emerges. Notable differences among these ring current maps include the highly uniform diatropic currents in C@Al_6Na_4, while the current density vectors beneath the Al–Cu bonds in C@Al_6Cu_4 and the current density vectors beneath the Al–Ag bonds in C@Al_6Ag_4 exhibit weaker intensity, which becomes even more attenuated and disturbed in C@Al_6Au_4. These results are consistent with the aforementioned conclusions that all of these C@Al_6M_4 species exhibit aromatic character, although it becomes weaker in the Ag-substituted system and is weakest in the Au-substituted one.

To further verify the existence of the magic number of 26 attributed to the non-hybridized bonding of the C atom, we consider further the stability of the O_h isomer of C@Si_6^{2+} and C@Ge_6^{2+}. Each unit exhibits six imaginary frequencies with the highest imaginary frequency for C@Si_6^{2+} being −156 cm^{-1}, and the highest imaginary frequency for C@Ge_6^{2+} reduced to −82 cm^{-1}. In contrast, the O_h isomer of C@Sn_6^{2+} is a truly stable isomer. A global structural search confirms that the O_h C@Sn_6^{2+} isomer is indeed the most stable one, with the next lower-lying isomer having an energy 10 kcal mol^{-1} higher than **Sn^{2+}·1** in terms of relative energy (*cf.* Fig. 6), with **Sn^{2+}** used as an abbreviation for CSn_6^{2+}. This result highlights the importance of the metallic nature of the element forming the cluster in alignment with the jellium model. Here, the Sn atom possesses a significantly greater metallicity as compared to Si and

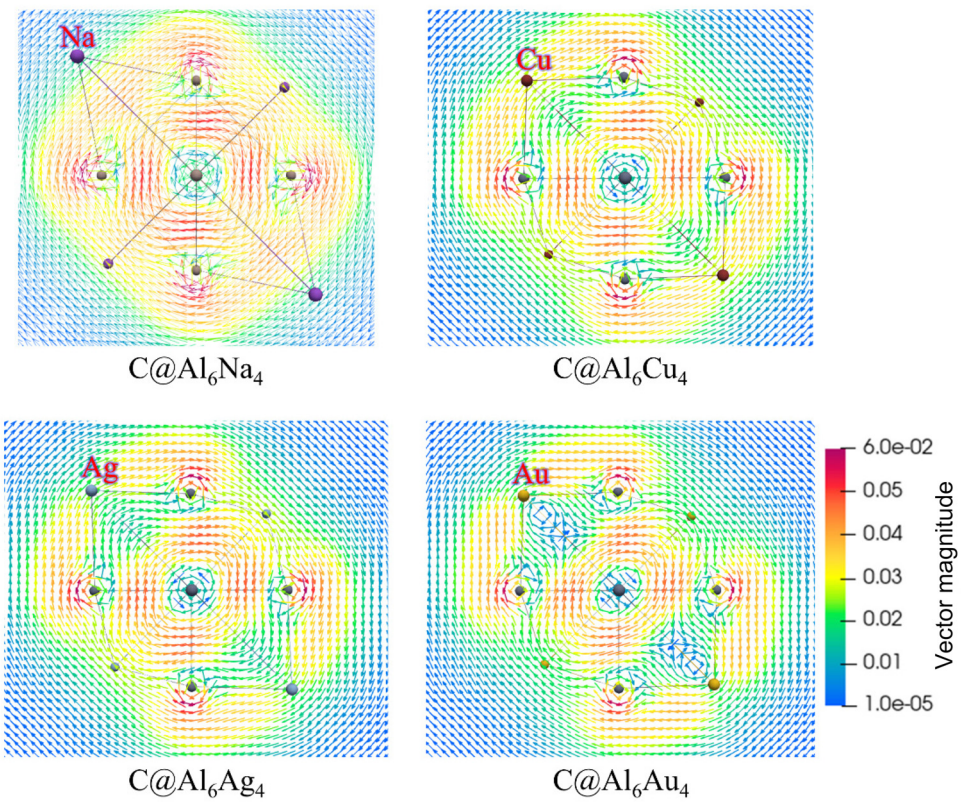

Fig. 5 GIMIC maps of C@Al_6M_4 were calculated on a plane situated 1 Bohr above the O_{xy} plane, with the magnetic field applied in the direction of the positive *z*-axis, perpendicular to the plane and pointing outward.

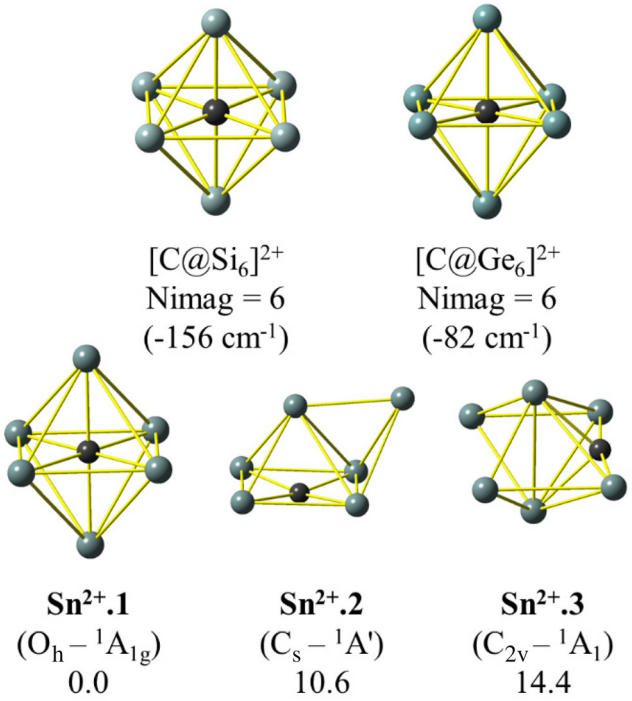

Fig. 6 Relaxed geometries of O_h $C@Si_6^{2+}$, $C@Ge_6^{2+}$, and the three lowest-lying CSn_6^{2+} isomers. The number of imaginary frequencies (N_{imag}) and the highest imaginary frequency for O_h $C@Si_6^{2+}$ and $C@Ge_6^{2+}$ are provided. Relative energies (kcal mol^{-1}) are obtained with ZPE corrections without scaling at the PBE/def2-TZVPPD level.

Ge. Similarly, the higher metallicity of Al with respect to that of B helps us understand the reason why Al_6^{2-} is stable with 20 electrons in the jellium model, whereas B_6^{2-} is not.[60]

Given the widespread synthesis of gold clusters,[6–9,13,14,21] which are generally more stable than their Ag and Cu counterparts at specific magic numbers, our study presents contrasting results. These findings may open up opportunities to replace more expensive coinage metals with their more affordable counterparts. Because tin-based clusters have also been extensively synthesized,[61] we thus anticipate that the $[C@Sn_6]^{2+}$ cluster can be synthesized in the near future to experimentally validate the magic number of 26.

4 Concluding remarks

The carbon atom participates in chemical bonding with other elements through the sp, sp^2, or sp^3 hybridization, resulting in its well-known maximal coordination number of four. The possibility of carbon bound to other atoms without undergoing hybridization is an existing phenomenon; however, it has not yet been generalized into a conceptual framework that allows its broader recognition and understanding. In structures such as $[C@Au_6]^{2+}$ or $C@Al_6Na_4$ clusters the C atom forms non-hybridized bonds with surrounding atoms. This non-hybridized bonding enables C to establish up to six bonds with neighboring atoms, and it is referred to as a hexavalent non-hybridized carbon atom. In the present study, we replaced Na with coinage metals and observed a higher stability for **Cu·1**, while **Au·1** exhibited significantly lower stability, and the stability of **Ag·1** was closer to that of **Na·1**. Although both Na and coinage metal atoms are expected to donate a single electron to the framework to form a polarized molecule, only Na exhibits such behavior in the **Na·1** structure. Coinage metals tend to donate electrons in a manner that brings their total donation close to that of the Al atoms. Of the coinage metals, gold (Au) is the least willing to donate electrons, leading to its isomers having the lowest stability. **Cu·1** can be regarded as a special case; all AO-fragment pairs exhibit positive OPDOS values, indicating their bonding overlaps. In contrast, negative OPDOS values in other isomers are in line with reduced stability. Nevertheless, all these structures are characterized by an aromatic character, due to a complete filling of all electron shells.

Furthermore, the magic number of 26, which is rather unusual within the jellium model, is validated through the optimal structures of $C@Al_6M_4$ and $C@Sn_6^{2+}$. The existence of the magic number of 26 in these structures can be explained by the significantly lower energy of the 2P shell as compared to the 1F shell. In the jellium model, these two electron shells are typically close in energy. The deeper energy level of the 2P shell, relative to the 1F shell, arises because (i) the 1F shell is shifted higher than usual due to its requirement for multi-layered molecular structures or the use of AOs with many nodal planes, and (ii) the C atom utilizes its nearly filled 2p orbitals to enhance its bonding in the 1P and 2P MOs. Overall, the present study not only introduces new molecules such as $C@Al_6M_4$ and $C@Sn_6^{2+}$ that possess a perfect hexa-coordinate C center, but also proposes a novel concept of the hexavalent non-hybridized carbon atom, and provides us with a rationale for the new magic number of 26 based on their intrinsic characteristics.

The bonding overlap between both the (p)C orbital and 1P orbital of the $[Au_6]^{2+}$ framework is a key parameter in enhancing the stability associated with the magic number of 8. Similarly, the overlap between the (p)C orbital and the 1P and 2P orbitals in the Al_6M_4 framework leads to the emergence of the magic number of 26. Variation in the stability of clusters with a magic number of 26 is attributed to the degree of bonding or antibonding overlap among these atomic/molecular orbitals.

Data availability

The data supporting this article have been included as part of the ESI.†

Conflicts of interest

The authors declare no conflict of interest.

Acknowledgements

LVD and MTN are thankful to the Van Lang University.

References

1 A. C. Castro, M. Audiffred, J. M. Mercero, J. M. Ugalde, M. A. Méndez-Rojas and G. Merino, *Chem. Phys. Lett.*, 2012, **519–520**, 29–33.
2 S. Li, C. Miao and G. Ren, *Eur. J. Inorg. Chem.*, 2004, **2004**, 2232–2234.
3 J.-C. Guo, L.-Y. Feng, X.-Y. Zhang and H.-J. Zhai, *J. Phys. Chem. A*, 2018, **122**, 1138–1145.
4 Y. Pei, W. An, K. Ito, P. von R. Schleyer and X. C. Zeng, *J. Am. Chem. Soc.*, 2008, **130**, 10394–10400.
5 V. T. Ngan and M. T. Nguyen, *J. Phys. Chem. A*, 2010, **114**, 7609–7615.
6 F. Scherbaum, A. Grohmann, B. Huber, C. Krüger and H. Schmidbaur, *Angew. Chem., Int. Ed. Engl.*, 1988, **27**, 1544–1546.
7 X.-L. Pei, P. Zhao, H. Ube, Z. Lei, K. Nagata, M. Ehara and M. Shionoya, *J. Am. Chem. Soc.*, 2022, **144**, 2156–2163.
8 X.-L. Pei, P. Zhao, H. Ube, Z. Lei, M. Ehara and M. Shionoya, *Nat. Commun.*, 2024, **15**, 5024.
9 O. Steigelmann, P. Bissinger and H. Schmidbaur, *Angew. Chem., Int. Ed. Engl.*, 1990, **29**, 1399–1400.
10 T. H. Maugh, *Science*, 1983, **222**, 403–403.
11 W. Ekardt, *Phys. Rev. B: Condens. Matter Mater. Phys.*, 1984, **29**, 1558–1564.
12 J. Tang, C. Zhang, N. Du, Y. Zhao and H. Chen, *Int. J. Quantum Chem.*, 2019, **119**, e25871.
13 F. Scherbaum, B. Huber, G. Müller and H. Schmidbaur, *Angew. Chem., Int. Ed. Engl.*, 1988, **27**, 1542–1544.
14 F. Scherbaum, A. Grohmann, G. Müller and H. Schmidbaur, *Angew. Chem., Int. Ed. Engl.*, 1989, **28**, 463–465.
15 D. I. Bezuidenhout, C. Esterhuysen, L. Dobrzańska, S. Cronje and H. G. Raubenheimer, *Z. Naturforsch., B*, 2024, **79**, 549–577.
16 S. Reimann, M. Koskinen and H. Häkkinen, *Phys. Rev. B: Condens. Matter Mater. Phys.*, 1997, **56**, 12147–12150.
17 T. Tsukamoto, N. Haruta, T. Kambe, A. Kuzume and K. Yamamoto, *Nat. Commun.*, 2019, **10**, 3727.
18 T. N. Gribanova, R. M. Minyaev, V. I. Minkin and A. I. Boldyrev, *Struct. Chem.*, 2020, **31**, 2105–2128.
19 E. Zeller, H. Beruda and H. Schmidbaur, *Inorg. Chem.*, 1993, **32**, 3203–3204.
20 Y. Yang and P. R. Sharp, *J. Am. Chem. Soc.*, 1994, **116**, 6983–6984.
21 D. Zhang, J. Dou, D. Li and D. Wang, *J. Coord. Chem.*, 2007, **60**, 825–831.
22 C. Zhang, M. Ding, Y. Ren, A. Ma, Z. Yin, X. Ma and S. Wang, *Nanoscale Adv.*, 2023, **5**, 3287–3292.
23 D. Grandjean, E. Coutiño-Gonzalez, N. T. Cuong, E. Fron, W. Baekelant, S. Aghakhani, P. Schlexer, F. D'Acapito, D. Banerjee, M. B. J. J. Roeffaers, M. T. Nguyen, J. Hofkens and P. Lievens, *Science*, 2018, **361**, 686–690.
24 A. Muñoz-Castro and R. B. King, *J. Phys. Chem. C*, 2017, **121**, 5848–5853.
25 H.-F. Zhang, M. Stender, R. Zhang, C. Wang, J. Li and L.-S. Wang, *J. Phys. Chem. B*, 2004, **108**, 12259–12263.
26 F. Fetzer, N. Pollard, N. C. Michenfelder, M. Strienz, A. N. Unterreiner, A. Z. Clayborne and A. Schnepf, *Angew. Chem., Int. Ed.*, 2022, **61**, e202206019.
27 P. V. Nhat and T. B. Tai, *Chem. Phys. Lett.*, 2018, **706**, 127–132.
28 A. E. Kuznetsov, A. I. Boldyrev, H.-J. Zhai, X. Li and L.-S. Wang, *J. Am. Chem. Soc.*, 2002, **124**, 11791–11801.
29 H. T. Pham, L. V. Duong, B. Q. Pham and M. T. Nguyen, *Chem. Phys. Lett.*, 2013, **577**, 32–37.
30 M. A. Addicoat and G. F. Metha, *J. Comput. Chem.*, 2009, **30**, 57–64.
31 J. H. Holland, *Adaptation in Natural and Artificial Systems: An Introductory Analysis with Applications to Biology, Control, and Artificial Intelligence*, MIT Press, 1992.
32 J. P. Perdew, A. Ruzsinszky, G. I. Csonka, L. A. Constantin and J. Sun, *Phys. Rev. Lett.*, 2009, **103**, 026403.
33 B. P. Pritchard, D. Altarawy, B. Didier, T. D. Gibson and T. L. Windus, *J. Chem. Inf. Model.*, 2019, **59**, 4814–4820.
34 C. Lee, W. Yang and R. G. Parr, *Phys. Rev. B: Condens. Matter Mater. Phys.*, 1988, **37**, 785–789.
35 B. Miehlich, A. Savin, H. Stoll and H. Preuss, *Chem. Phys. Lett.*, 1989, **157**, 200–206.
36 A. D. Becke, *J. Chem. Phys.*, 1993, **98**, 5648–5652.
37 K. Raghavachari, G. W. Trucks, J. A. Pople and M. Head-Gordon, *Chem. Phys. Lett.*, 1989, **157**, 479–483.
38 P.-Å. Malmqvist and B. O. Roos, *Chem. Phys. Lett.*, 1989, **155**, 189–194.
39 K. Andersson, P. Malmqvist and B. O. Roos, *J. Chem. Phys.*, 1992, **96**, 1218–1226.
40 *GIMIC, version 2.0*, a current density program. Can be freely downloaded from **https://github.com/qmcurrents/gimic**.
41 J. Jusélius, D. Sundholm and J. Gauss, *J. Chem. Phys.*, 2004, **121**, 3952–3963.
42 T. Lu and F. Chen, *J. Comput. Chem.*, 2012, **33**, 580–592.
43 T. Lu, *J. Chem. Phys.*, 2024, **161**, 082503.
44 E. D. Glendening, C. R. Landis and F. Weinhold, *J. Comput. Chem.*, 2019, **40**, 2234–2241.
45 F. Neese, F. Wennmohs, U. Becker and C. Riplinger, *J. Chem. Phys.*, 2020, **152**, 224108.
46 M. J. Frisch, G. W. Trucks, H. B. Schlegel, G. E. Scuseria, M. A. Robb, J. R. Cheeseman, G. Scalmani, V. Barone, G. A. Petersson, H. Nakatsuji, X. Li, M. Caricato, A. V. Marenich, J. Bloino, B. G. Janesko, R. Gomperts, B. Mennucci, H. P. Hratchian, J. V. Ortiz, A. F. Izmaylov, J. L. Sonnenberg, D. Williams-Young, F. Ding, F. Lipparini, F. Egidi, J. Goings, B. Peng, A. Petrone, T. Henderson, D. Ranasinghe, V. G. Zakrzewski, J. Gao, N. Rega, G. Zheng, W. Liang, M. Hada, M. Ehara, K. Toyota, R. Fukuda, J. Hasegawa, M. Ishida, T. Nakajima, Y. Honda, O. Kitao, H. Nakai, T. Vreven, K. Throssell, J. A. Montgomery Jr.,

J. E. Peralta, F. Ogliaro, M. J. Bearpark, J. J. Heyd, E. N. Brothers, K. N. Kudin, V. N. Staroverov, T. A. Keith, R. Kobayashi, J. Normand, K. Raghavachari, A. P. Rendell, J. C. Burant, S. S. Iyengar, J. Tomasi, M. Cossi, J. M. Millam, M. Klene, C. Adamo, R. Cammi, J. W. Ochterski, R. L. Martin, K. Morokuma, O. Farkas, J. B. Foresman and D. J. Fox, *Gaussian 16, Revision C.01*, Gaussian, Inc., Wallingford CT, 2019.

47 N. Shen, Y. Fan and S. Pamidighantam, *J. Comput. Sci.*, 2014, **5**, 576–589.

48 R. Dooley, K. Milfeld, C. Guiang, S. Pamidighantam and G. Allen, *J. Grid Comput.*, 2006, **4**, 195–208.

49 Q. Du, X. Wu, P. Wang, D. Wu, L. Sai, R. B. King, S. J. Park and J. Zhao, *J. Phys. Chem. C*, 2020, **124**, 7449–7457.

50 J. M. Bakker, J. Jalink, D. Dieleman and A. Kirilyuk, *J. Phys.: Condens. Matter*, 2018, **30**, 494003.

51 H. Baek, J. Moon and J. Kim, *J. Phys. Chem. A*, 2017, **121**, 2410–2419.

52 D. A. Götz, R. Schäfer and P. Schwerdtfeger, *J. Comput. Chem.*, 2013, **34**, 1975–1981.

53 Y. A. Jeilani, L. V. Duong, O. M. S. Al Qahtani and M. T. Nguyen, *Phys. Chem. Chem. Phys.*, 2024, **26**, 11347–11359.

54 P. Alayoglu, S. C. Rathnayaka, T. Chang, S. G. Wang, Y.-S. Chen and N. P. Mankad, *Chem. Sci.*, 2024, **15**, 13668–13675.

55 J. V. Davis, L. Stevens, S. M. DeCarlo, D. H. Mayo, P. Y. Zavalij, C. J. Snyder and B. W. Eichhorn, *Eur. J. Inorg. Chem.*, 2024, **27**, e202300695.

56 H. Yang, Y. Zhang and H. Chen, *J. Chem. Phys.*, 2014, **141**, 064302.

57 T. J. Lee and P. R. Taylor, *Int. J. Quantum Chem.*, 2009, **36**, 199–207.

58 T. Zhou, L. Ma, J. Tang and H. Chen, *Chem. Phys. Lett.*, 2020, **739**, 137026.

59 K. Clemenger, *Phys. Rev. B: Condens. Matter Mater. Phys.*, 1985, **32**, 1359–1362.

60 M. T. Huynh and A. N. Alexandrova, *J. Phys. Chem. Lett.*, 2011, **2**, 2046–2051.

61 R. Kimmich and A. Schnepf, *Dalton Trans.*, 2024, **53**, 17429–17436.